ELSEVIER

Contents lists available at ScienceDirect

Environmental Modelling & Software

journal homepage: www.elsevier.com/locate/envsoft



Object-based correction of LiDAR DEMs using RTK-GPS data and machine learning modeling in the coastal Everglades



Hannah M. Cooper^{a,*}, Caiyun Zhang^b, Stephen E. Davis^c, Tiffany G. Troxler^d

- ^a Department of Geography, Planning, and Environment, East Carolina University, A-204 Brewster, Greenville, NC, 27858, USA
- b Department of Geosciences, Florida Atlantic University, 777 Glades Road, Boca Raton, FL, 33431, USA
- ^c Everglades Foundation, 18001 Old Cutler Rd. Palmetto Bay, FL, 33157, USA
- ^d Southeast Environmental Research Center, Florida International University, 11200 SW 8th Street, Miami, FL, 33199, USA

ARTICLE INFO

Keywords: LiDAR Object-based image analysis Machine learning Monte Carlo DEMs Coastal wetlands

ABSTRACT

Light Detection and Ranging (LiDAR) Digital Elevation Models (DEMs) are frequently applied in modeling coastal environments. We present an object-based correction approach for accurate and precise DEMs by integrating LiDAR point data, aerial imagery, and Real Time Kinematic-Global Positioning Systems. Four machine learning techniques (Random Forest, Support Vector Machine, k-Nearest Neighbor, and Artificial Neural Network) were compared with the commonly used bias-correction method. The Random Forest object-based model produced best predictions for two study areas: Nine Mile (Mean Bias Error (MBE) reduced 0.18 to $-0.02\,\mathrm{m}$, Root Mean Square Error (RMSE) reduced 0.22 to 0.08 m) and Flamingo (MBE reduced 0.17 to 0.02 m, RMSE reduced 0.24 to 0.10 m). A Monte Carlo model was developed to combine errors into the object-based machine learning corrected DEMs, and uncertainty maps spatially revealed the likelihood of error. The object-based correction approach provides an attractive alternative to the bias-correction method.

1. Introduction

1.1. Significance of LiDAR Digital Elevation Models (DEMs) in the coastal Everglades

A unique federal/state partnership in the USA is making efforts to restore the original Everglades ecosystem, which has been largely modified in the past century by human activities (NRC, 2014). Everglades restoration requires better Digital Elevation Models (DEMs) with a vertical Root Mean Square Error (RMSE) less than 0.15 m to monitor and simulate water levels, water depths, and hydroperiods (Jones et al., 2012). For the coastal Everglades, DEMs are also recommended to have a fine spatial resolution (e.g. 5 m) to identify local areas vulnerable to coastal hazards such as sea-level rise and hurricanes (Zhang, 2011; Cooper et al., 2015).

Current available elevation datasets in the coastal Everglades include the National Elevation Dataset (NED), Shuttle Radar Topography Mission (SRTM), High Accuracy Elevation Database (HAED), and Light Detection and Ranging (LiDAR). The vertical error of the 30 m NED and SRTM datasets are 0.48–1.89 m and 4.01 m in terms of the RMSE (Gesch et al., 2014), respectively, which are insufficient for restoration requirements (Jones et al., 2012). The Everglades hydrologic

community has agreed upon the vertical elevation error threshold of 0.15 m for restoration projects (Desmond, 2003; Jones et al., 2012), which is interpreted here as the RMSE. To meet this strict error specification, the U.S. Geological Survey (USGS) conducted a region-scale survey from 1995 to 2007 using an Airborne Height Finder (AHF) with differential Global Positioning System (GPS) to measure sub-water and terrain surface elevation. Elevation data collected in this airborne survey were combined with the ground survey data to generate a DEM dataset known as HAED in the Everglades. The vertical error of HAED meets the restoration requirements; however, its coarse spatial resolution (400 m) limits its applications in coastal areas.

To generate fine spatial resolution DEMs in the coastal Everglades, the Florida Division of Emergency Management collected LiDAR data over Florida's coastal areas. LiDAR has been recognized as a standard to generate fine spatial resolution DEMs for various applications (Jensen, 2015). However, it is a challenge for LiDAR to obtain accurate DEMs in coastal marsh environments due to several combined factors that include the complexity of coastal marshes, instrument, and software. Coastal marshes in the Everglades are typically inundated with murky water containing dark peat soils, which make the automated ground elevation measures difficult. LiDAR often fails to penetrate through dense marsh plants, preventing the system (instrument) from discerning

E-mail address: cooperh18@ecu.edu (H.M. Cooper).

^{*} Corresponding author.

true ground returns from non-ground returns (i.e. vegetation). In addition, the common software used by vendors are commonly not effective at filtering LiDAR mass points into ground returns for marsh vegetated areas (Morris et al., 2005; Rosso et al., 2006; Schmid et al., 2011).

1.2. Coastal marsh LiDAR DEM correction

LiDAR DEMs have shown to overestimate marsh ground elevations as much as 0.65 m (Medeiros et al., 2015), and errors tend to grow with both increasing vegetation density and marsh height (Rosso et al., 2006; Sadro et al., 2007; Schmid et al., 2011). To address this issue, a binning procedure was utilized to generate binning DEMs because the bias and error can be reduced considerably (Rosso et al., 2003; Schmid et al., 2011; Medieros et al., 2015; Buffington et al., 2016). Researchers typically apply corrections to an already generated LiDAR DEM using field surveyed Real Time Kinematic (RTK)-GPS data (Schmid et al., 2011; Hlaldik and Alber, 2012; Medieros et al., 2015; McClure et al., 2016; Buffington et al., 2016). RTK-GPS is an alternative technique for collecting accurate elevation data through field surveys. The application of RTK-GPS data has been recognized as a standard to assess and calibrate LiDAR DEMs. The uncertainty of LiDAR DEMs in marsh environments is mainly attributable to vegetation and tends to be speciesdependent. Therefore, one method in marsh LiDAR DEM correction using RTK-GPS data focuses on a solution to derive a bias specific to each species, and then correct the LiDAR DEM cell by cell using the species-dependent bias (e.g., Hlaldik and Alber, 2012; McClure et al., 2016). This is referred to as the grid-based bias-correction method in this study. This type of correction assumes that errors in the LiDAR DEM are spatially consistent within a species, and the heterogeneous structure of this species has not been considered. LiDAR uncertainty in marsh environments is influenced by the characteristics of plants, which present a varying elevation within a species rather than a constant (Rogers et al., 2016, 2018). A second method in LiDAR DEM correction uses above ground biomass and vegetation indices with linear modeling techniques (Medeiros et al., 2015; Buffington et al., 2016). While this type of correction considers the heterogenous structure within a species, it assumes that the underlying data follow a normal distribution, which may not always the case. Therefore, a nonparametric approach that incorporates the spatial heterogeneity of LiDAR uncertainty and has the potential to enhance the integrity of LiDAR DEMs in marsh environments has been developed in this study.

1.3. Object-based nonparametric modeling techniques in LiDAR correction and DEM generation

One strategy to include the heterogeneity of LiDAR uncertainty in the correction is to identify the relationship between marsh characteristics and LiDAR uncertainty. LiDAR statistical metrics have proven useful to characterize vegetation in the Florida Everglades (Zhang, 2014). A quantification of the relationship between LiDAR measurements and RTK-GPS data might be an effective alternative to the commonly used bias-correction method. LiDAR statistical metrics can be derived at the grid level with a regular size and shape or the object level with varying sizes and shapes. Object-based modeling and mapping is more valuable than grid-based methods in the Everglades because coastal managers and planners are more interested in a region/ patch rather than an individual grid/raster (Zhang et al., 2018). Objectbased Image Analysis (OBIA) provides the unique opportunity to develop an object-based LiDAR correction approach to be reported and tested in this study. OBIA has been well developed and widely used in image classification, as reviewed by Blaschke (2010). However, OBIA has never been applied in correcting LiDAR DEMs or LiDAR point data. This study is the first to explore the potential of OBIA for LiDAR correction and generating LiDAR DEMs by developing an object-based correction approach.

A recent study from Rogers et al. (2018) shows that LiDAR-derived measurements tend to be nonlinearly related to LiDAR uncertainty, suggesting nonparametric machine learning modeling algorithms might be more effective than traditional linear modeling techniques in LiDAR correction. In this study, we examined four nonparametric machine learning modeling algorithms for LiDAR correction and DEM generation: Random Forest (RF), Support Vector Machine (SVM), k-Nearest Neighbor (k-NN), and Artificial Neural Network (ANN). These algorithms have shown to perform well in marsh characterization and biomass modeling in the Everglades (Zhang, 2014; Zhang et al., 2018).

1.4. Monte Carlo uncertainty simulation

Since corrected DEMs approximate the true elevation, they too contain vertical inaccuracies and errors that need considering. The vertical accuracy of a DEM refers to how close the modeled elevations are to the true elevations of an independent data source of better accuracy (i.e. RTK-GPS). Vertical error or uncertainty in DEMs may be expressed numerically by standard deviation (σ), which is a measure of precision that represents a range of errors around the mean (accuracy) between the DEM and RTK-GPS. Common sources of LiDAR DEM vertical accuracy and error, and the standards used to assess them, are provided in a review by Cooper et al. (2013). Adjusting for the uncertainty in the underlying data respective to the DEMs is especially important for low slope marsh environments where a difference of a few centimeters in elevation can impact the results of rigorous ecological and hydrological modeling. Unfortunately, the effect of uncertainty in DEMs is often neglected and consequently not adjusted for by DEM providers and users (Wechsler and Kroll, 2006). Monte Carlo simulation techniques provide the unique opportunity where the effect of the uncertainty related to the underlying data in LiDAR corrected DEMs can be observed and adjusted. Monte Carlo is a statistical approach useful for modeling dynamic geographic phenomena with significant uncertainty such as DEMs (e.g., Wechsler and Kroll, 2006). It has been widely used in mapping and modeling of coastal marsh environments such as the probabilistic estimation of sea-level rise marine inundation (Cooper and Chen, 2013; Clough et al., 2016) and groundwater inundation (Cooper et al., 2015), carbon emissions (Henman and Poulter, 2008), and intertidal habitats on barrier islands (Enwright et al., 2018). However, it has not been applied in adjusting corrected DEMs by considering the underlying error estimates in the correction procedure. In principle, Monte Carlo simulation follows the law of large numbers theorem where averaging the results over many trials provides a more reliable result of the expected value (Graham and Talay, 2013). In this study, we extended the Monte Carlo DEM uncertainty approach by Wechsler and Kroll (2006) to consider the vertical accuracy and errors in the corrected DEMs, RTK-GPS data and benchmarks, and vertical datums to which the data are vertically referenced. It is expected that by combining Monte Carlo simulation with the corrected DEMs and error estimates, the approximations of the true elevations being modeled are more reliable for end users' needs.

1.5. Objectives

The main objective of this study is to develop an object-based LiDAR correction approach for generating corrected DEMs to complement the existing bias-correction methods by combining OBIA and machine learning modeling techniques. The specific objectives are to: 1) explore the pros and cons of object-based machine learning LiDAR correction method compared with the current grid-based bias-correction methods; 2) examine the potential benefits of object-based elevation data over the grid-based raster DEMs, and 3) adjust for the effect of uncertainty in the final corrected DEM deliverables and produce maps where the likelihood of object-based corrected DEM uncertainty can be observed.

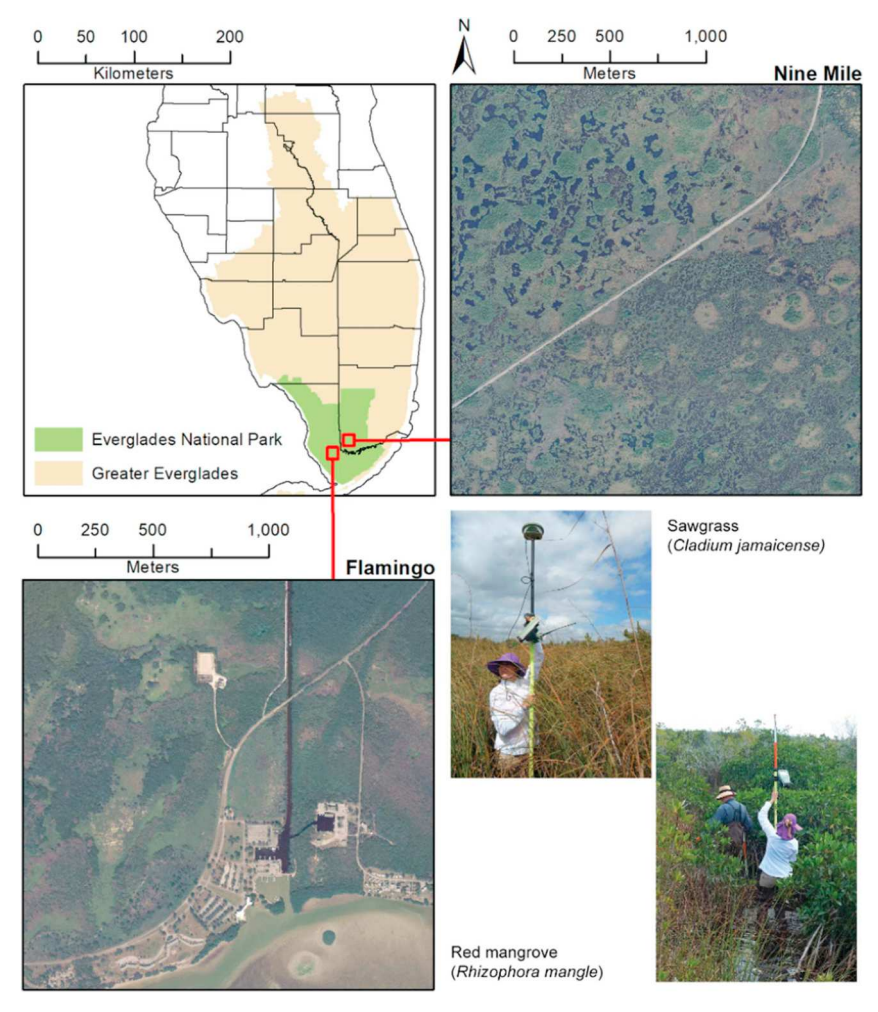


Fig. 1. Map of the two study sites in the southern coastal region of Everglades National Park.

2. Study area and data

2.1. Study area

The study area is in the southern coastal region of Everglades National Park (ENP) (Fig. 1). We surveyed two sites of this area for collecting RTK-GPS data in this study. The first site is located just below the Nine Mile Pond turnoff from Main Park Road (hereinafter referred to as Nine Mile; ~1 km2 in area) This site is historically a freshwater marsh dominated by sawgrass (Cladium jamaicense). The second site is in the southernmost headquarters of ENP and includes the Flamingo Visitor Center (hereinafter referred to as Flamingo; ~3 km² in area). This site is dominated by high-density tall stands of trees (taller than 5 m) including red mangrove (Rhizophora mangle), black mangrove (Avicennia germinans), white mangrove (Laguncularia racemosa), and buttonwood (Conocarpus erectus). During the survey, the ecological impact of hurricanes could be seen within the plant communities at each study site. In Nine Mile, low density trees with heights less than 5 m are pervasive including red mangrove and buttonwood. This is because winds from hurricanes Donna (1960) and Betsy (1965) resulted in the establishment of red mangrove (Rhizophora mangle) seedlings in Nine Mile, thus the red mangrove does not require its intertidal habitat to survive (Lodge, 2010). In Flamingo, the inland movement of mud during hurricanes resulted in a patchwork of coastal prairies where dominant species include saltwort (Batis maritima), glasswort (Salicornia spp.), and saltgrass (Distichlis spicata), all generally less than 1 m tall. The soils for Nine Mile are dominated by sawgrass peat deposits, while the soils for Flamingo vary spatially and are dominated by mangrove peat deposits and hurricane deposited marl. Both study sites are underlain by highly permeable Miami limestone, which makes up part of the Biscayne Aquifer. Water flows towards the southwest where extensive freshwater diversions due to current water management practices coupled with rising sea levels are threatening the stability of the coastal peat marshes.

2.2. Data

Data sources used in this study include RTK-GPS ground elevation data for correcting LiDAR elevations, LiDAR for building object-based corrected DEMs, and aerial imagery for generating image objects. For our RTK-GPS survey data collection, a reconnaissance was performed to identify the survey sites and existing survey controls. Survey sites were selected based on roadside access to different vegetation communities. After the reconnaissance, we collected RTK-GPS elevation data in February and March 2016, the dry season of South Florida (November-May), to be seasonally consistent with the acquisition of LiDAR and aerial imagery. In the data collection, existing survey controls were chosen based on their vicinity to our study sites, unobstructed view of the sky, accessibility, and horizontal and vertical orders that affect the overall error of the survey. Three National Geodetic Survey (NGS) benchmarks were used in the field: NGS tidal benchmark PID AB2404, NGS benchmarks PID AC4648, and PID AC4659, which were reported to have a horizontal and vertical classification of first-order, class II, with a maximum elevation difference error of 0.07 m (1 standard deviation or σ) (https://www.ngs.noaa.gov/ datasheets/). The Leica 1200 system was utilized with reported real

time errors of 0.01 m in the horizontal and 0.02 m in the vertical (RMSE at 68% confidence interval) (Leica Geosystems, 2008). The Leica 1200 base receiver was set up over the NGS and tidal benchmarks. A topo shoe was fitted to the survey rods of the moving receivers or rovers to prevent sinking into the peat soils. Elevations were surveyed near low tide with nominal precisions $\leq 0.01 \, \mathrm{m}$ in horizontal and $\leq 0.03 \, \mathrm{m}$ in vertical positions (RMSE at 68% confidence interval). Survey data were collected for each dominant vegetation community to provide a representation of the overall population and with a separation radius greater than or equal to 2 m. In total, we collected 483 RTK-GPS ground elevations (132 for Nine Mile; 351 for Flamingo) which were vertically referenced to North American Vertical Datum of 1988 (NAVD88) using Geoid 12A.

The current best available LiDAR data for the study area were collected by the Florida Division of Emergency Management in February 2008 using the Leica ALS50 Airborne Laser Scanner system, which was reported to have a horizontal error of 0.07-0.64 m (1 standard deviation or 1 σ) and vertical error of 0.08–0.24 m (1 σ) after post-processing (Leica Geosystems, 2007). The data are available at National Oceanic and Atmospheric Administration (NOAA)'s data access viewer (https:// coast.noaa.gov/dataviewer). Although intensity images are also available, they were not used in this study for model simplicity. The average LiDAR point density reported is 2 points/m² for unobscured areas (no trees or buildings). The vendor filtered the LiDAR point cloud into classified ground (bare-earth) and non-ground returns (vegetation, structures, and buildings). RTK-GPS (Trimble 4700 and Trimble 4000 series) and total station surveys were also conducted by the vendor for LiDAR accuracy assessment in July 2007 for Nine Mile and in December 2007 for Flamingo, which were also considered in this study. Since both the LiDAR and vendor's survey data were vertically referenced to the NAVD88 using Geoid 03, we transformed their LiDAR and RTK-GPS data to be consistent with our RTK-GPS data using a vertical datum transformation tool from NOAA (https://vdatum.noaa.gov/).

Fine spatial resolution aerial photography with three spectral channels (red, green, and blue) is available for both sites. The Nine Mile aerial imagery was collected in January 2016 with a spatial resolution of 0.25 m, while the Flamingo imagery was collected in January 2012 with a spatial resolution of 0.30 m. We used the aerial imagery to produce image objects for conducting object-based LiDAR correction and DEM modeling.

3. Methodology

3.1. Framework of the object-based machine learning LiDAR correction and DEM generation

We designed a framework for conducting object-based machine learning LiDAR correction and DEM generation, as shown in Fig. 2. In the framework, image objects were produced first using an image segmentation approach, then LiDAR statistical metrics were extracted for each object to be used for ground elevation modeling and prediction. Field RTK-GPS elevation data were spatially matched at the object level to the LiDAR measurements to be used for model development. A training dataset was used to fine tune the parameters of four machine learning regression algorithms (RF, SVM, k-NN, and ANN) before making predictions on the new LiDAR measurements to generate the object-based LiDAR corrected DEMs. An independent test dataset was then used to quantitatively compare the object-based LiDAR corrected DEMs that were then combined with Monte Carlo simulation to account for the uncertainty in the underlying data. The major steps in the framework include image segmentation, data matching, machine learning modeling LiDAR correction and DEM generation, accuracy assessment, and Monte Carlo uncertainty simulation. These steps are provided in the following subsections.

3.1.1. Image segmentation

We generated objects from the aerial imagery using the multiresolution segmentation algorithm in eCognition Developer 9.3 (Benz et al., 2004; Trimble, 2017). The algorithm first segments individual pixels of an image before merging neighboring segments together until a heterogeneity threshold is reached (Benz et al., 2004). The heterogeneity threshold is determined by user-defined parameters including scale, color/shape and smoothness/compactness weights. The scale is an arbitrary value allowing for a relative comparison between different scales. The scale determines the size of objects where a smaller scale value produces smaller homogeneous objects, and a larger scale value produces larger heterogenous objects. In this study, a smaller scale is reasonable for restoration planning and sea-level rise mapping which requires highly detailed elevation products. To help identify an optimal scale for generating the best prediction model, we tested three segmentations using scale parameters ranging from 20 to 40 at an interval of 10. The color/shape parameter was set to 0.9/1.0 for all three bands so that spectral information was weighted most heavily for segmentation. The smoothness/compactness parameter was set to 0.5/0.5 for all three bands so that compact and non-compact segments were favored equally. After segmentation, the LiDAR elevation statistical metrics (minimum, mean, maximum, standard deviation, range and count or number of LiDAR points) were extracted for each image object to be used as independent variables for ground elevation modeling and mapping. Objects without LiDAR measurements were dropped for further analysis. The LiDAR statistical metrics were derived using the original LiDAR point elevations which have proven more valuable than the application of a raster layer generated from LiDAR data for extracting LiDAR measurements (Zhang et al., 2011, 2014).

3.1.2. Data matching

It is common for researchers to match the observed RTK-GPS measures with individual LiDAR DEM grid cells to calculate correction factors. In this study, we spatially matched our RTK-GPS data (132 for Nine Mile; 351 for Flamingo) with the LiDAR measurements at the object level. We expected two advantages from the object-based matching scheme. First, it can reduce the uncertainty of positional discrepancy between LiDAR measures and field RTK-GPS data. Second, a "pure" object/region is more representative for the plant structure and/or DEM than any individual grid cell within this object/region. OBIA offers the capability to match the field RTK-GPS data to relatively homogeneous objects with a varying shape and size, rather than a grid cell in which plants might be heterogeneous in structure.

3.1.3. Object-based nonparametric machine learning modeling and LiDAR correction and DEM generation

In this study, we examined four nonparametric machine learning algorithms (RF, SVM, k-NN, and ANN) for ground elevation modeling with RTK-GPS data as the dependent variable and LiDAR measurements as the independent variables. RF is an ensemble learning technique developed by Breiman (2001) to improve the classification and regression tree method. Advantages of RF include its speed and capability to deal with complex relationships between predictors, but it requires many training samples that should be representative (Belgiu and Dragut, 2016). SVM is a statistical learning approach that looks for an optimal hyperplane to minimize training errors. An advantage to SVM is its capability to produce improved estimations based on a small number of training samples, but parameter issues may arrive with this algorithm (Mountrakis et al., 2011). k-NN is an instance-based learning method that searches for the best match to denote inputs. An advantage of k-NN is its capability to make local approximations while simultaneously solving multiple problems and dealing with changes in the problem domain; however, it requires the selection of an appropriate distance metric to combine neighbors for predictions (Chirici et al., 2016). ANN models data based on the structure of neurons and the synapses of human brains. ANN can generalize in a noisy environment,

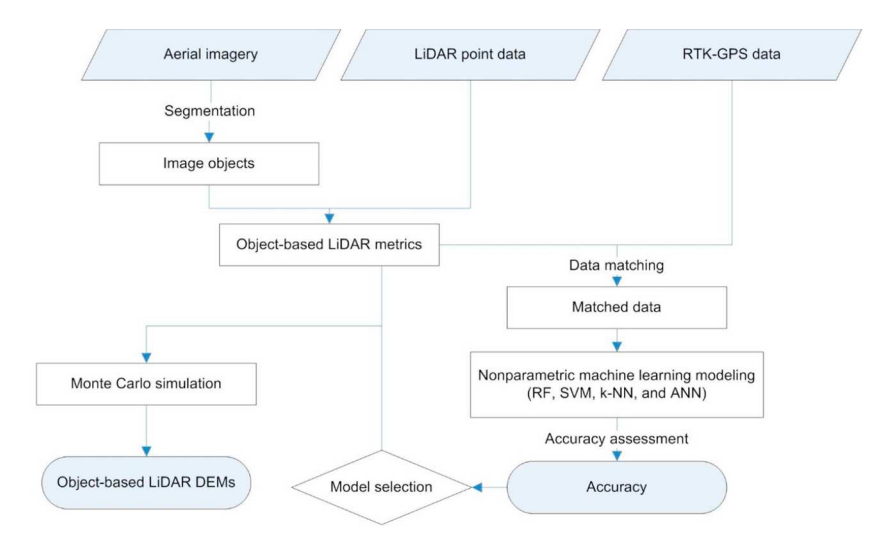


Fig. 2. Framework for object-based LiDAR correction and DEM generation.

but it may be difficult to interpret because the inner workings are like a black box (Mas and Flores, 2008). Since each model has its own pros and cons, the potential of each for LiDAR correction has been explored in this study.

The 132 matched samples for Nine Mile and 351 matched samples for Flamingo were randomly split into two datasets with one to train the machine learning models used to correct the LiDAR measurements before generating DEMs, and the other to test the predictive performance of all finalized models used to generate corrected DEMs. The National Digital Elevation Program (NDEP, 2004) recommends a minimum of 30 checkpoints to access the vertical accuracy of elevation data. We chose to randomly select a total of 30 samples as test data samples used to assess the vertical accuracy of the corrected DEMs for the Nine Mile and Flamingo study areas, respectively. The remaining samples (102 for Nine Mile; 321 for Flamingo) were used to train and fine tune the models' parameters.

To help reduce overfitting, training time, and improve model accuracy, automatic attribute selection is useful for determining the most relevant explanatory variables. The supervised attribute selection filter in WEKA version 3.8 (Hall et al., 2009) was used to select relevant explanatory variables for use in model construction. The filter evaluates the value of a subset of explanatory variables by considering the individual predictive ability of each variable along with the degree of redundancy between them (Hall, 1998). The relevant explanatory variables for the Nine Mile object-based dataset were all LiDAR measurements except standard deviation and range, and the relevant explanatory variables for the Flamingo object-based dataset were LiDAR minimum and count. We employed WEKA version 3.8 (Hall et al., 2009) where the training datasets were used to fit the four machine learning regression algorithms over different tuning parameters using resampling techniques. The RF algorithm (Breiman, 2001) was utilized where the following tuning parameters were defined: 1) the number of decision trees in the forest, and 2) the number of randomly selected variables subsetted from the total number of variables that are used for each node split in a tree. The kernel, precision, and penalty parameters were adjusted when using the SVM algorithm (Shevade et al., 1999). The k-NN algorithm (Aha and Kibler, 1991) was evaluated by fine tuning distance measures, weighted functions, and k value parameters. The parameters fit for the ANN multilayer perceptron algorithm (Mas and Flores, 2008) were the learning rate and number of hidden layers and training cycles. Repeatability was achieved by using the same sequence of random numbers where the seed was set to 123 for all applicable model runs. For each of the four machine learning techniques, the tuning parameters were chosen based on trial and error using the

lowest RMSE provided by 10-fold cross validation. The finalized models were then utilized to make predictions on new LiDAR measurements. Using ArcGIS version 10.4 (http://www.esri.com/) Data Management tools, the prediction attribute features were spatially joined to the object-based features based on their spatial relationship to generate the object-based LiDAR corrected DEMs.

3.1.4. Accuracy assessment

The test data were used to produce quantitative assessments of the final corrected DEMs to compare between models, choose which models produced the best results, and perform Monte Carlo simulations. The association between each corrected DEM's model-predicted (P) values and observed (O) RTK-GPS measures were evaluated using several correlation, difference, and summary measures. One type of correlation measure was calculated. The correlation or degree of association between P and O was expressed as Pearson's coefficient of correlation (r). Three types of difference measures were calculated. Estimates of the average error were described as the Mean Absolute Error (MAE) and RMSE. Any systematic error that makes all estimates off by a certain amount, or bias, was described as the Mean Bias Error (MBE). Several summary measures were then calculated. These include the mean (μ) and standard deviation (σ). These indices were calculated by:

$$r = \frac{\sum_{i=1}^{n} (P_i - \overline{P_i})(O_i - \overline{O_i})}{\sqrt{\sum_{i=1}^{n} (P_i - \overline{P_i})^2} \sqrt{\sum_{i=1}^{n} (O_i - \overline{O_i})^2}}$$
(1)

$$MAE = \frac{\sum_{i=1}^{n} |P_i - O_i|}{n}$$
 (2)

$$RMSE = \sqrt{\frac{\sum_{i=1}^{n} (P_i - O_i)^2}{n}}$$
 (3)

$$MBE = \frac{\sum_{i=1}^{n} (P_i - O_i)}{n}$$
 (4)

where P_i is the model-predicted value, $\overline{P_i}$ is the mean of the model-predicted values, O_i is the observed value, $\overline{O_i}$ is the mean of the observed values, n is the number of matched test data samples, and i is an integer from 1 to n.

3.1.5. Monte Carlo uncertainty simulation on corrected DEMs

Before we can adjust for the effect of uncertainty in the final corrected DEM deliverables and produce maps where the likelihood of corrected DEM uncertainty can be illustrated, the vertical accuracy and error in the underlying data along with their distributions needs

considering. These uncertainties included the following: 1) vertical datums and any transformations made between them, 2) RTK-GPS measurements, 3) vertical benchmarks used in survey, and 4) the model predictions for each object in the object-based corrected DEMs. First, the errors associated with the vertical datum to which the data are referenced were obtained from NOAA (2013). The σ is used to quantify uncertainties for vertical datums, where NOAA considers a constant σ of 5 cm for NAVD88 nationwide. No transformations between datasets were needed for this study to include transformation errors. Second, the RTK-GPS measurements contained a vertical RMSE ≤0.03 m (RMSE = 1σ), while the vertical benchmarks to which the surveys were based is 0.07 m (1 σ). It is assumed that the individual uncertainties are independent where the value of one measurement does not affect the value of the other measurement and are randomly distributed following a normal distribution. This allows for the total uncertainty of the RTK-GPS measures and vertical benchmarks to be calculated by the root sum of squares as the Maximum Cumulative Uncertainty (MCU) σ:

$$MCU_{\sigma} = \sqrt{\sigma_1^2 + \sigma_2^2 + \dots \sigma_N^2}$$
 (5)

Finally, the accuracy and error in the corrected DEMs were calculated in the previous section, which are needed for the Monte Carlo simulation.

To adjust for the uncertainty related to the underlying data, Monte Carlo simulation is applied to our corrected DEMs having a single output quantity (more reliable elevation) where the input quantities (survey, vertical datums and model predictions) are characterized by any specific Probability Distribution (PD). We did not apply filtered error fields in the procedure (e.g. Wechsler and Kroll, 2006; Enwright et al., 2018); instead, unfiltered error fields were considered as a worst-case scenario of the effects of corrected DEM uncertainty (Wechsler and Kroll, 2006). We reduce the equation by Cooper and Chen (2013) to consider the uncertainty related to our corrected DEMs:

$$DEM_{reliable} = \sum (DEM_{survey} + DEM_{datum} + DEM_{error} + DEM_{x,y})/n$$
 (6)

where $DEM_{reliable}$ is a final object-based corrected DEM value that is more reliable provided the uncertainty in the underlying data; DEM_{survey} is a random variable sampled proportional to the RTK-GPS measures and vertical benchmarks survey data distribution; DEM_{datum} is a random variable sampled proportional to the vertical datum distribution; DEM_{error} is a random variable sampled proportional to the model predictions; and $DEM_{x,y}$ is a constant elevation z value of an object at an x,y location. The sampling procedure is repeated a total of 1000 cases for each object. An illustration of the Monte Carlo-based elevation uncertainty model is shown in Fig. 3.

To produce maps that spatially illustrate the likelihood that a corrected DEM is in error, it is assumed that the "true" elevation is best represented by the corrected DEM derived from the most accurate model. In this way, the likelihood that a corrected DEM value is in error is based on the probability that the corrected DEM value deviates from

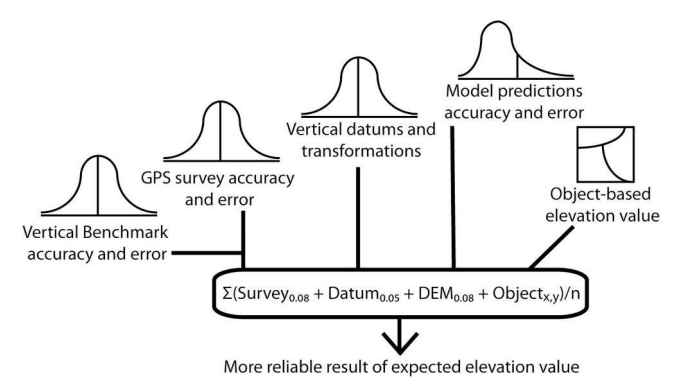


Fig. 3. Illustration of the Monte Carlo-based elevation uncertainty model.

the true elevation. Monte Carlo simulation is applied to our objectbased corrected DEMs having a single output quantity (likelihood of error) where the input quantities (survey, vertical datums and model predictions) are characterized by any specific Probability Distribution (PD) using the following equation:

$$Likelihood_{error} = \sum ((DEM_{survey} + DEM_{datum} + DEM_{error} + DEM_{x,y}) < (DEM_{survey} + DEM_{datum} + True_{error} + True_{x,y}))/n$$
(7)

where the difference from equation (6) is that $Likelihood_{error}$ is the probability an object-based corrected value deviates from the True elevation, $True_{error}$ is a random variable sampled from the most accurate object-based corrected DEM, and $True_{x,y}$ is a constant elevation z value at an x,y location derived from the most accurate object-based corrected DEM. Although any ranking scheme can be utilized, we chose to generalize the likelihood of error values using the following ranking scheme where object-based probability values ranging from 0 to 0.39 are assigned equal to low, object-based probability values ranging from 0.4 to 0.59 are assigned equal to medium, and object-based probability values ranging from 0.6 to 1 are assigned equal to high likelihood of error. The generalized object-based likelihood layers are then used to calculate total land area susceptible to error for each ranking scheme (low, medium, high).

3.2. Grid-based nonparametric machine learning modeling and LiDAR correction and DEM generation

For comparison purposes, we also conducted the grid-based LiDAR correction and DEM generation. The process was first implemented in Python version 2.7.10 (https://www.python.org/) using ArcGIS Arcpy Python site package to create an easy workflow. First, three grids with resolutions ranging from 1 to 3 m at an interval of 1 m were generated. The minimum resolution was chosen based on the reported LiDAR average point density of 2 pts/m². The binning technique was then utilized (Rosso et al., 2003; Schmid et al., 2011; Medieros et al., 2015; Buffington et al., 2016) to assign a grid cell's center point the respective LiDAR statistic (minimum, mean, maximum, standard deviation, range, count) when more than one LiDAR attribute falls within that cell. If only one LiDAR attribute falls within a cell, that attribute is assigned to that cell (null assigned to no data). Due to the nature of the landscape consisting of dense coastal vegetation and surface-water with dark peat soils below making LiDAR measures sometimes difficult, certain cells contained null values. The results were a total of six raster datasets for Nine Mile and six raster datasets for Flamingo, each containing LiDAR minimum, mean, maximum, standard deviation, range and count per respective grid cell. The relevant explanatory variables for the Nine Mile grid-based dataset were all LiDAR measurements except standard deviation, range and count, and the relevant explanatory variables for the Flamingo grid-based dataset were simply the LiDAR mean and minimum. The process presented in section 3.1.3 above was then repeated to generate grid-based corrected DEMs.

3.3. BIN and BIN bias-correction DEM generation

Since LiDAR ground returns are known to overestimate coastal marsh elevations, the minimum bin technique (hereinafter simply referred to as BIN) seems more reasonable than interpolation methods for our two study sites when comparing the bias-correction procedure with the four machine learning regression algorithms. Here, the grid-based and object-based datasets containing the minimum LiDAR value are referred to as the grid-based and object-based BIN. It is common for researchers to calibrate grid-based LiDAR DEMs with bias correction factors (Schmid et al., 2011; Hladik and Alber, 2012; McClure et al., 2016). For comparison purposes, the grid-based and object-based BIN

Table 1

Descriptive statistics for each experiment. Where BIN = minimum binning, BIN bias-correction = BIN calibrated by the respective mean bias, RF = Random Forest, SVM = Support Vector Machine (SVM), k-NN = k-Nearest Neighbor, ANN = Artificial Neural Network, \bar{P} = the mean of the model-predicted values, \bar{O} = the mean of the observed RTK-GPS, $\sigma_{P-\bar{O}}$ = the standard deviation of the differences between \bar{P} and \bar{O} , MBE = mean bias error between model-predicted and RTK-GPS, MAE = Mean Absolute Error, RMSE = Root Mean Square Error between model-predicted and RTK-GPS, r = coefficient of correlation, n = number of RTK-GPS, all in meters (except n). The $\sigma_{P-\bar{O}}$ and MBE were used in Monte Carlo simulation. Experiments in bold are selected as demonstrating the best performance.

Nine Mile object-based scale 30												
Experiment	n	Ō	$ar{P}$	$\sigma_{ar{P}-ar{O}}$	MBE	MAE	RMSE	r				
Uncorrected LiDAR	30	-0.13	0.06	0.13	0.18	0.19	0.22	0.65				
BIN	169	-0.10	0.05	0.17	0.03	0.12	0.17	0.76				
BIN bias-	30	-0.13	-0.14	0.16	-0.04	0.12	0.16	0.05				
correction												
RF	30	-0.13	-0.15	0.07	-0.02	0.05	0.08	0.70				
SVM	30	-0.13	-0.15	0.08	-0.02	0.06	0.08	0.69				
k-NN	30	-0.13	-0.15	0.07	-0.02	0.05	0.08	0.68				
ANN	30	-0.13	-0.14	0.08	-0.01	0.06	0.08	0.55				
Nine Mile grid-based 3 m												
Uncorrected LiDAR	30	-0.13	0.11	0.13	0.24	0.24	0.27	0.77				
BIN	102	-0.09	0.05	0.20	0.14	0.17	0.25	0.75				
BIN bias-	30	-0.13	-0.01	0.13	-0.03	0.11	0.13	0.59				
correction												
RF	30	-0.13	-0.14	0.06	-0.01	0.05	0.06	0.76				
SVM	30	-0.13	-0.13	0.09	-0.01	0.06	0.09	0.46				
k-NN	30	-0.13	-0.15	0.07	-0.02	0.05	0.07	0.70				
ANN	30	-0.13	-0.17	0.09	-0.04	0.07	0.10	0.41				
Flamingo object-based scale 30												
Uncorrected LiDAR	30	0.10	0.27	0.17	0.17	0.17	0.24	0.84				
BIN	211	0.29	0.29	0.23	0.00	0.14	0.23	0.88				
BIN bias-	N/A	N/A	N/A	N/A	N/A	N/A	N/A	N/A				
correction												
RF	30	0.10	0.12	0.10	0.02	0.06	0.10	0.95				
SVM	30	0.10	0.01	0.09	-0.01	0.15	0.09	0.69				
k-NN	30	0.10	0.15	0.14	0.05	0.10	0.14	0.92				
ANN	30	0.10	0.13	0.13	0.03	0.09	0.13	0.93				
Flamingo grid-	based 3	3 m										
Uncorrected LiDAR	30	0.10	0.27	0.15	0.17	0.17	0.22	0.87				
BIN	321	0.29	0.40	0.26	0.11	0.18	0.28	0.83				
BIN bias- correction	30	0.10	0.22	0.14	0.00	0.10	0.14	0.88				
RF	30	0.10	0.03	0.30	-0.08	0.16	0.30	0.25				
SVM	30	0.10	0.00	0.28	-0.09	0.17	0.29	0.40				
k-NN	30	0.10	0.03	0.31	-0.08	0.17	0.31	0.17				
ANN	30	0.10	0.05	0.25	-0.05	0.15	0.25	0.66				

datasets were also calibrated by the Mean Bias Error (MBE) calculated from the training datasets (102 for Nine Mile; 321 for Flamingo). These datasets are referred to as the grid-based and object-based BIN biascorrection.

4. Results

4.1. Grid-based vs. object-based corrected DEMs

To compare the bias-correction method with machine learning modeling, descriptive statistics are displayed in Table 1. In reviewing the summary position parameter or average of predictions (\bar{P}), the BIN

and BIN bias-correction techniques tend to systematically overestimate the corresponding observed average of observations (\bar{O}) to a higher degree than the machine learning techniques with one exception: The Flamingo object-based scale 30 BIN dataset suggests that \bar{P} and \bar{O} are the same (Table 1). Therefore, the bias-correction technique cannot be applied to the Flamingo object-based scale 30 BIN because the difference parameter MBE is zero. Machine learning techniques provide a valuable alternative to the bias-correction approach when LiDAR data contains no systematic bias (i.e. MBE = 0.0) and is less unprecise (e.g. $\sigma = 0.23$ m).

The difference measures (MAE, RMSE) and MBE help to better determine which modeled grid-based 3 m resolution and modeled object-based scale 30 datasets are preferred (Table 1). In terms of the MAE and RMSE for Nine Mile, a meaningful distinction can be made between the BIN bias-based and machine learning experiments. The MAE and RMSE are lowest (best) for the object-based and grid-based machine learning experiments at the Nine Mile study site. In reviewing the MBE, the machine learning experiments also reduce the bias when compared to the bias-correction procedure. Further examination of r indicates that the Nine Mile grid-based 3 m RF has a slightly higher degree of association between P and O (r = 0.76) when compared to the object-based scale 30 RF (r = 0.70). Overall, the RF algorithm performed best for the Nine Mile grid-based and object-based datasets when compared to the bias-correction technique.

In terms of the MAE and RMSE for Flamingo, a slightly different distinction can be made between the BIN bias-correction and machine learning experiments. The MAE and RMSE are lowest (best) for the object-based machine learning experiments where RF performs best overall at the Flamingo study site. However, the grid-based machine learning experiments did not perform as well as the grid-based BIN bias-correction experiment at the Flamingo study site. The examination of r indicates that the Flamingo object-based scale 30 RF has a slightly higher degree of association (r=0.95) when compared to the grid-based BIN bias-correction (r=0.88). Overall, the object-based RF algorithm performed best compared to all other experiments for the Flamingo study site.

We also compared the RTK-GPS measurements with the uncorrected LiDAR ground return elevations within an object-based or grid-based dataset (Table 1). The LiDAR systematically overestimates the ground for both study sites. For Nine Mile, the uncorrected LiDAR within an object demonstrated a lower MBE of $0.18\,\mathrm{m}$ and RMSE of $0.22\,\mathrm{m}$ when compared to the uncorrected LiDAR within a grid (MBE = $0.24\,\mathrm{m}$; RMSE = $0.27\,\mathrm{m}$). Although the standard deviation of $0.13\,\mathrm{cm}$ is the same for both the object-based and grid-based datasets, the RMSE may be more useful because it demonstrates that large errors are present in the MAE. This is because the RMSE calculation assigns higher weights to larger errors by first squaring the errors before taking their average. For Flamingo, no meaningful distinction can be made between the uncorrected LiDAR within an object (MBE = $0.17\,\mathrm{m}$; RMSE of $0.24\,\mathrm{m}$) when compared to the uncorrected LiDAR within a grid (MBE = $0.17\,\mathrm{m}$; RMSE = $0.22\,\mathrm{m}$).

4.2. Grid-based and object-based DEM mapping

The corrected DEM maps were derived by applying the machine learning models to the object-based scale 30 and grid-based 3 m data for each of the two study sites. This provided the opportunity to incorporate the uncertainty in the underlying data into the final corrected DEM products using equation (6) with Monte Carlo simulations (see Figs. 4 and 5). In the maps, red represents higher elevations above NAVD88 and blue represents lower elevations below NAVD88, all in meters. For both study areas, the object-based corrected DEM maps qualitatively do a better job at estimating unknown locations when compared to the grid-based corrected DEM maps. This is illustrated by the missing data values shown in white that are more prevalent in the grid-based corrected DEM maps. The Flamingo study site also has more

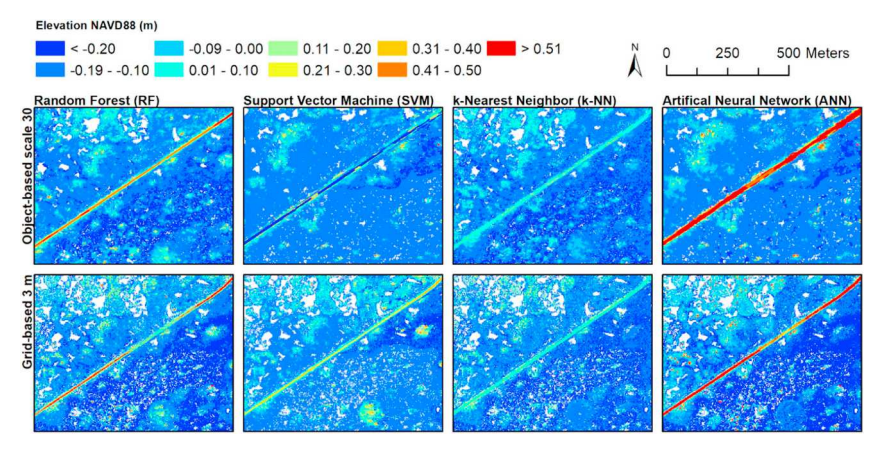


Fig. 4. Final Monte Carlo object-based and grid-based corrected DEMs for Nine Mile. White areas denote no data.

topographic variation than the Nine Mile study site allowing for better visual examination of the object-based and grid-based experimental results. The corrected DEM maps show that the object-based approach provides a more detailed account of the ground elevation values when compared to the grid-based corrected DEM maps (see Fig. 5 for more variation in the graduated colors). The corrected DEM maps also demonstrate that the object-based corrected DEMs are more representative of the landscape.

4.3. Uncertainty mapping relative to the best model

The final uncertainty maps that illustrate the probability that an object-based corrected elevation value is in error from the true elevation are shown for the Nine Mile and Flamingo study areas in Figs. 6 and 7, respectively. Although the Nine Mile and Flamingo object-based RF corrected DEMs do not represent an unbiased result, they were considered as the true elevation because they achieved the best result when compared to all other object-based machine learning models. The Nine Mile and Flamingo object-based RF corrected DEMs were used to calculate the likelihood of corrected DEM uncertainty using equation (7). In the maps, the likelihoods that SVM, k-NN, and ANN object-based corrected elevations are in error from the true elevations (i.e., RF object-based corrected elevations) are represented by a ranking scheme of blue for low, green for medium, and red for high chance of error. Although the Nine Mile maps in Fig. 6 illustrate that the likelihood of error varies from each experiment, it is difficult to qualitatively assess

the preferred approach from these maps alone. On the other hand, the Flamingo maps shown in Fig. 7 clearly illustrate the ANN object-based corrected DEM has the lowest likelihood of error, while the k-NN object-based corrected DEM has the highest likelihood of error. Table 2 compliments the uncertainty maps by providing a quantitative assessment of the total area that is in likelihood of error. For Nine Mile, the ANN object-based corrected DEM contains the largest area with a low likelihood of uncertainty (20% of total land area) and smallest area with a high likelihood of uncertainty (12% of total land area) making it the preferred approach. Overall, the uncertainty maps and complimentary table help DEM users to qualitatively and quantitatively assess the uncertainty of an object-based corrected elevation.

5. Discussion and conclusions

5.1. Machine learning regression for LiDAR correction

After conducting a thorough literature review, we found one recent study that used machine learning modeling in marshes to develop a LiDAR correction approach (Rogers et al., 2018). These authors recommended that this type of modeling be extended to other regions with different vegetation types to examine its robustness. In this study, the potential of four machine learning regression algorithms (RF, SVM, k-NN, and ANN) were examined to correct LiDAR elevation data in the coastal Everglades for two study sites: 1) Nine Mile dominated by sawgrass marsh and mangrove swamp, and 2) Flamingo dominated by

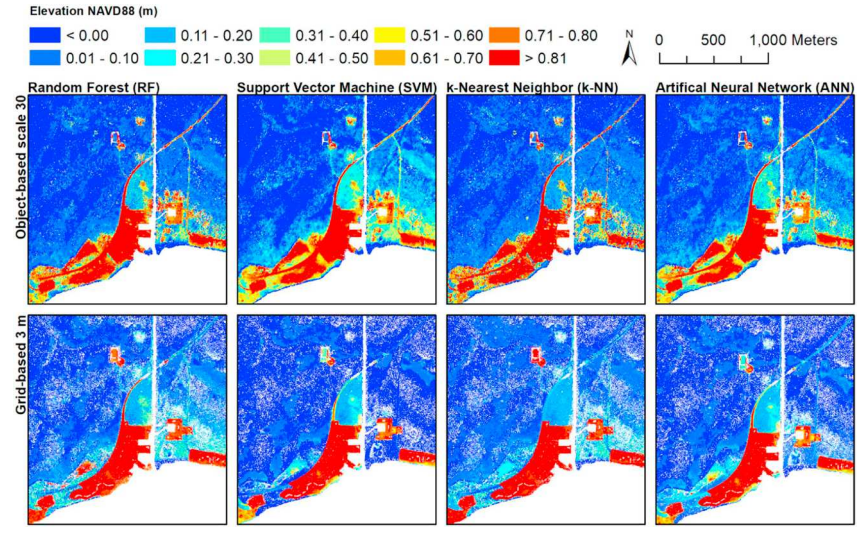


Fig. 5. Final Monte Carlo object-based and grid-based corrected DEMs for Flamingo. White areas denote no data.

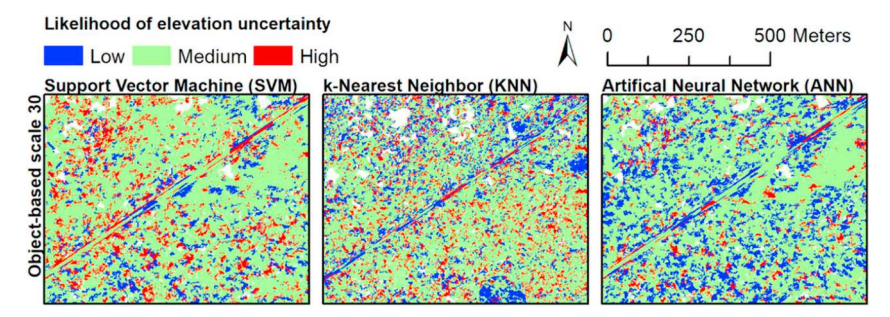


Fig. 6. Monte Carlo-based likelihood maps of corrected DEM uncertainty for Nine Mile.

mangrove swamp and coastal prairies. All algorithms produced an acceptable degree of association between the predicted and observed values where the coefficient of correlation (r) is over 0.55 using objectbased modeling. RF performed best for the Nine Mile object-based modeling (r = 0.70) where the uncorrected LiDAR MBE was reduced from 0.18 to -0.02 m, MAE was reduced from 0.19 to 0.05 m, standard deviation (o) was reduced from 0.13 to 0.07 m, and RMSE was reduced from 0.22 to 0.08 m. RF also performed best for the Flamingo objectbased modeling (r = 0.95) where the uncorrected LiDAR MBE was reduced from 0.17 to 0.02 m, MAE was reduced from 0.17 to 0.06 m, standard deviation (σ) was reduced from 0.17 to 0.10 m, and RMSE was reduced from 0.24 to 0.10 m. Although the vegetation communities, explanatory variables of importance, and number of RTK-GPS are not the same, our results are comparable with the study by Rogers et al. (2018) where RF performed best for discrete LiDAR where all marsh vegetation MBE = -0.01 cm; standard deviation and RMSE = 0.11 cm. Based on this study and the study by Rogers et al. (2018), the RF algorithm is robust when correcting discrete LiDAR elevation data for the two regions with their own unique vegetation communities.

The RF algorithm seems to handle well datasets that do not follow a Gaussian distribution, contain a bias, and are highly spatially autocorrelated, which is typical of marsh environments. This is likely due to the nature of the RF algorithm injecting randomness in the variables and averaging over many predictions to get an unbiased model result with low variance (see Criminisi et al., 2011 for a review on RF). However, RF is not without weaknesses. When using RF for regression, the model does not do a good job at predicting beyond the range of the training data, which may have an impact on our results depending on how well the LiDAR and RTK-GPS measurements represent the overall population.

Since it is known that DEMs generated using interpolation results in additional error, and due to the nature of the LiDAR overestimating the true ground due to vegetation and open water, we decided against using interpolation. Instead, a binning procedure to correcting LiDAR elevations known as the minimum binning (BIN) approach was utilized because it has shown to reduce bias and error in marsh environments

when compared to interpolation (Rosso et al., 2003; Schmid et al., 2011; Medeiros et al., 2015; Buffington et al., 2016). A few case studies have also demonstrated that the bias-correction technique does a satisfactory job at improving the bias (e.g. Hladik and Alber, 2012; McClure et al., 2016). It was anticipated that by combining the BIN and bias-correction techniques into a BIN bias-correction object-based procedure, the bias and error could be further improved for comparison with the machine learning object-based modeling. However, this was not the case for our Nine Mile study site where the BIN bias-correction object-based dataset MBE was slightly increased from 0.03 to −0.04 cm and the change in the σ and RMSE was negligible (0.17–0.16 cm) when compared to the BIN object-based dataset. Rogers et al. (2016) pointed out that while the bias-correction technique typically does well in correcting for bias, machine learning techniques provide a better option for error removal. In this study, the RF object-based modeling improved bias and significantly lowered error when compared to the BIN and BIN bias-correction techniques.

5.2. Grid-based vs object-based LiDAR correction and DEM generation

Researchers have focused on correcting LiDAR DEMs at the grid level (e.g., Schmid et al., 2011; Hlaldik and Alber, 2012; McClure et al., 2016; Buffington et al., 2016; Rogers et al., 2016). A thorough literature review revealed that no other efforts have been made for applying OBIA in object-based LiDAR correction nor applying OBIA in modeling LiDAR DEMs at the object level. The object-based LIDAR correction approach developed and tested in this study successfully combines the spatial features of fine spatial resolution aerial imagery (≤0.30 m) with lowposting density (≤2 pts/m²) LiDAR elevation measurements making it an attractive alternative to the commonly used grid-based method. The object-based technique's ability to take advantage of spatial features within an image to define an object/patch and predict more area where LiDAR is sparse is attractive (see Figs. 4 and 5). This reduces the need for DEM void filling procedures. The object-based approach can also reduce positional discrepancy between the image and RTK-GPS measurements because an object represents a vegetation patch better than a

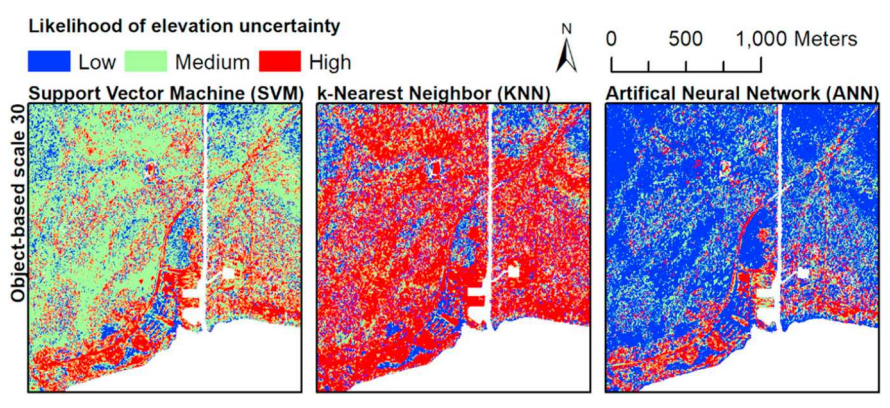


Fig. 7. Monte Carlo-based likelihood maps of corrected DEM uncertainty for Flamingo.

Table 2
Total area in likelihood of error.

Study area	Experiment	Low		Medi	um	High	
		Area km ²	% area	Area km²	% area	Area	% area
Nine Mile	SVM	0.10	13	0.57	74	0.10	13
	KNN	0.13	17	0.51	66	0.13	17
	ANN	0.16	20	0.52	68	0.09	12
Flamingo	SVM	0.56	15	2.16	59	0.95	26
	KNN	0.85	23	0.87	24	1.95	53
	ANN	2.49	68	0.81	22	0.37	10

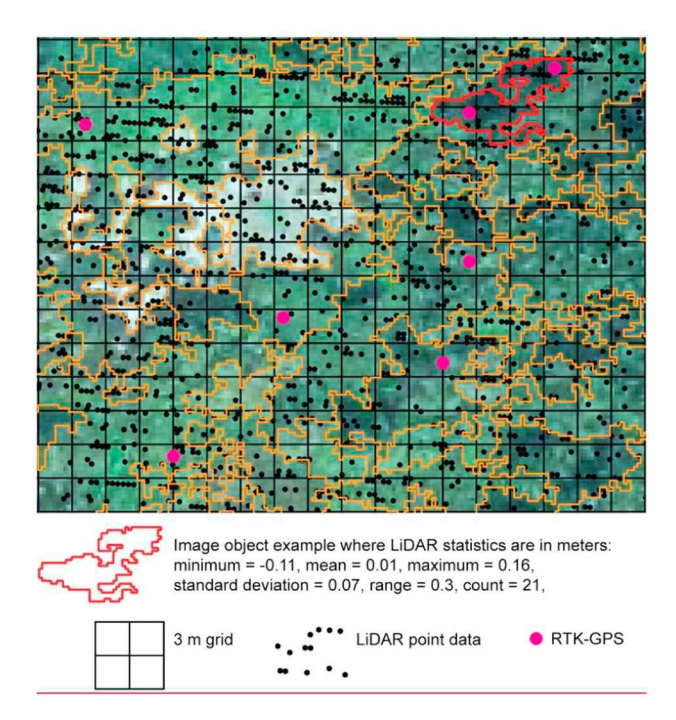


Fig. 8. Illustration of image objects derived from OBIA on the Flamingo imagery dataset.

single grid cell (Fig. 8). The object-based mapping and modeling reduces local noise in heterogeneous wetland environments by averaging the spectra of all pixels within an object (Dronova, 2015). In the Everglades, vegetation has a high spatial and spectral heterogeneity. The heterogeneity threshold is determined by a user-defined scale parameter. A smaller scale value produces smaller homogeneous patches of vegetation, while a larger scale value produces larger heterogenous patches. Additionally, a species typically presents a range of elevation uncertainty opposed to a constant (Rogers et al., 2016), so it is unlikely that an entire vegetation species would need a constant correction using the bias-correction technique (Rogers et al., 2018). The capability of the object-based LiDAR correction technique to reduce the spatial bias and uncertainty within each individual object/patch successfully addresses the issue where the assumption is made that the accuracy and error is the same for an entire vegetation community.

The inherent structure of vector data makes the object-based corrected DEMs attractive and convenient when manipulating and performing operations on elevation data. The vector object-based mapping in our case produced smoother elevation gradients and was geographically more accurate because an object is represented by the line features of a vegetation patch, whereas the raster grid-based mapping is represented by an artificial uniform grid size (Fig. 8). The mixed pixel problem is most apparent in the 2 m grid because it is assumed that a grid cell covers a homogeneous vegetation patch. Since the aerial imagery have a fine spatial resolution (0.25–0.3 m), it is easier to

interpret homogenous vegetation patches as objects from the fine resolution images (Fig. 8). Additionally, object-based elevations are stored as attribute tables allowing for flexibility in data manipulation such as joining tables. Since both data management and the integrity of object-based corrected elevations is maintained through topology rules, network and proximity operations are performed more efficiently. For example, network-based analytical tools used for solving complex routing issues in a GIS can easily be applied to object-based corrected DEMs to identify thresholds of dynamical marsh system response to water and nutrient fluxes. Proximity-based analytical tools can also be easily applied to an object-based corrected DEM to select by attributes and identify proximity to other features such as the shoreline. These vector-based operations are especially useful for assessing the impacts of sea-level rise and storm related events on natural and human coastal systems (e.g. Cooper et al., 2015).

Although the object-based technique provides some benefits in elevation mapping and modeling, it is not without its weaknesses. Here, we identify three limitations related to the scale parameter, vector data structure, and processing time. First, the scale parameter used for generating the size of objects can impact the object-based modeling results. A small scale produces homogenous objects, while a large scale produces more heterogenous objects. In this study, we tested several scale parameters by trial-and-error. Although methods exist for optimizing the scale parameters in image segmentation (e.g. Johnson and Xie, 2011), we did not apply them in this study. These techniques may help improve the results. Second, spatial analysis tools and filtering methods require raster data. To perform these operations, the Nine Mile object-based corrected DEM would need to be converted to a raster using the original 0.25 m resolution aerial imagery as its grid size and processing extent to maintain the integrity of the object-based corrected elevations. Although this requires an additional step, converting an object-based corrected DEM to a grid-based corrected DEM that matches the fine resolution imagery used to generate the objects may be useful for fine scale mapping of habitat and elevation loss due to the conversion of coastal peat marshes to inland open water from sea-level rise (i.e., peat collapse). Third, the object-based machine learning technique has a high computational intensity when compared to the MB bias-correction method. Although the object-based corrected DEMs provided the best results, the BIN bias-correction method may be more attractive to researchers that require a technique with a lower computation intensity.

Finally, it is interesting to re-note that although the MAE and RMSE are lowest (best) for the object-based machine learning experiments at the Flamingo study site, the grid-based machine learning experiments did not perform as well as the grid-based BIN bias-correction. We speculate that this may be due to the vegetation. The Flamingo study site is dominated by high-density tall stands of mangroves (taller than 5 m) making it difficult for the laser to penetrate to the ground. There are a limited number LiDAR classified ground returns within each 3 m grid cell. In this study, the machine learning techniques may produce better predictions for an object because there are generally more LiDAR returns within an object when compared to a grid cell.

5.3. Monte Carlo corrected DEM uncertainty mapping

Past research focuses on LiDAR DEM correction without including the effects of uncertainty in the corrected DEMs (e.g. Schmid et al., 2011; Hladik and Alber, 2012; Medieros et al., 2015; McClure et al., 2016; Buffington et al., 2016). Since vertical inaccuracies and/or errors remain in our corrected DEMs, we used Monte Carlo simulation to adjust for these effects in the final corrected DEM products and produced maps where the likelihood of error can be observed on an objectby-object basis. Researchers utilizing a sea-level rise bathtub approach that does not consider uncertainty in the underlying data (e.g. Zhang, 2011) would benefit from more reliable delineations of the inundation zones based on a corrected DEM that has been further adjusted by any underlying errors. The uncertainty maps and complimentary table allow DEM users to effectively evaluate which regions are prone to error for their intended application. For example, a researcher investigating freshwater marsh elevation loss due to saltwater intrusion may find the uncertainty maps useful in guiding additional field campaigns where it is more challenging for the remotely sensed data and machine algorithms to accurately predict elevations. Monte Carlo simulation has been widely used in mapping and modeling of coastal marsh environments. However, there has been limited application of this technique in adjusting for the inaccuracies and/or errors in corrected DEMs.

5.4. Error sources in LiDAR correction and DEM generation

Many sources of error impact the elevation estimation such as upscaling RTK-GPS data to objects, the geoid models and transformations relative the vertical datum to which the data are referenced, and time gaps between RTK-GPS, LiDAR, and aerial imagery acquisition. In our study, the RTK-GPS were upscaled from a single x,y point to an entire object's area. The RTK-GPS measurements were matched to the image objects of varying shapes and sizes. The spatial resolution of the aerial imagery for Nine Mile was 0.25 m and the minimum size of each object was 0.25 m², while the spatial resolution of the aerial imagery for Flamingo was 0.30 m and the minimum size of each object was 0.09 m². Therefore, it was assumed that the RTK-GPS measures represented the elevation of the entire object. Also, the LiDAR data were transformed from NAVD88 using Geoid 03 to NAVD88 using Geoid 12A. We considered a constant error for NAVD88 nationwide (NOAA, 2013) in the modeling; however, it is not clear how transforming between geoids may impact this error. This may lead to more uncertainties in the corrected DEMs. Finally, there were significant time gaps between the acquisition years of the current best available LiDAR, aerial imagery, and RTK-GPS field measurements. Variability in the vegetation and topography is largely controlled by season, hurricanes, and water management practices. South Florida's dry and rainy seasons will have an impact on vegetation growth and sediment shrinkage and swelling. All data utilized in this study were collected between January-March during the rainy season. Sediment accumulation will also have a minimal impact on elevation change between 2008 and 2016 because the elevation change is within the vertical error of 0.08-0.24 m of the LiDAR system (Leica Geosystems, 2007). For example, elevation change for Everglades mangroves was measured as $0.37 \pm 0.12 \,\mathrm{mm/yr}$ (Cahoon and Lynch, 1997). The maximum elevation change (0.37 + 0.12 = 0.49 mm) multiplied by the maximum number of (2016-2008 in years $0.49 \text{ mm} \times 8 \text{ yrs} = 3.92 \text{ mm}$. This 3.92 mm or 0.392 cm elevation change is within the LiDAR system's vertical error. A similar calculation can be made for Everglades sawgrass where elevation change was measured as 0.32 ± 0.04 mm/yr (Craft and Richardson, 1993). It should also be noted that no hurricanes hit the study area between 2008 and 2016, which would likely have had an impact on soil deposition and erosion and vegetation structure.

5.5. Orientation of future works

Although the developed object-based LiDAR correction approach was successful at estimating accurate and precise elevations in this study, the authors identify several suggestions for improvement of future works. The developed object-based LiDAR correction approach was tested on two sites consisting of coastal marsh, swamp, and prairie. Additional research is needed in other regions with coastal marsh and woody environments to examine the robustness of this technique. We tested several independent variables in the predictive modeling including six LiDAR elevation statistical metrics (minimum, mean, maximum, standard deviation, range and count). Future works should explore data fusion techniques that integrate multiple data sources in elevation correction. For example, additional object-based spatial features such as spectral features, texture, and inclusion of more LiDAR features such as intensity statistics and optical image features can be extracted for each object, which may have potential to improve the object-based LiDAR correction. We only tested the aerial imagery in the segmentation process when generating objects. However, the multiresolution segmentation algorithm in eCognition can also generate objects by integrating the LiDAR point cloud with aerial imagery. This may be advantageous when generating larger image objects by accounting for elevation gradients that may be observed in other areas, but this needs exploring. Additionally, we determined the RF objectbased model performed best for this study. However, ensemble analysis of comparable models may make the predictions more reliable than using an individual model. This should be explored in future works in elevation correction. It should be noted that we did not consider the spatial structure of error (e.g., Holmes et al., 2000) in the Monte Carlo modeling, which has potential to improve the reliability of the final corrected DEM products. This requires additional RTK-GPS measurements used in testing and needs exploring. We only compared errors spatially for each object-based machine learning approach to the best model as a reference. Restoration managers and planners may find useful the spatial distribution of errors for the best model. This also requires additional RTK-GPS measurements and should be explored in future works.

Finally, with the advancement of Unmanned Aerial Vehicles (UAVs) data acquisition in coastal environments (Klemas, 2015), and special approval by the National Park Service, simultaneous collection of all data sources during the same year and season is more achievable and may improve the results. Development of an object-based UAV-derived measurements approach has potential in elevation correction.

5.6. Conclusions

In this study, we developed an object-based LiDAR correction approach to modeling sawgrass marsh, mangrove swamp, and coastal prairie elevations by combining Object-based image analysis (OBIA), machine learning, and Monte Carlo techniques. The results suggested that this new approach was promising for elevation modeling and mapping compared to the bias-correction and grid-based modeling techniques. The authors draw the following conclusions from this study:

Machine learning regression techniques are effective at generating accurate and precise object-based Digital Elevation Models (DEMs). Four machine learning regression techniques were evaluated with the bias-correction technique: Random Forest (RF), Support Vector Machine (SVM), k-Nearest Neighbor (k-NN), and Artificial Neural Network (ANN). RF achieved the best result for the Nine Mile object-based modeling where the Mean Bias Error (MBE) was reduced from 0.18 to -0.02 m, standard deviation (σ) was reduced from 0.13 to 0.07 m, and Root Mean Square Error (RMSE) was reduced from 0.22 to 0.08 m. RF also performed best for the Flamingo object-based modeling where the MBE was reduced from 0.17 to 0.02 m, σ was reduced from 0.17 to 0.10 m, and RMSE was reduced from 0.24

to 0.10 m.

- The object-based LiDAR correction approach provides an attractive alternative to the commonly used grid-based modeling. The object-based approach has potential to reduce positional discrepancy between an image object and RTK-GPS measurement because an object better represents a vegetation patch than a single grid cell. The capability of the object-based modeling to reduce the spatial bias and uncertainty on an object-by-object basis successfully addresses the issue where the bias-correction technique assumes spatial bias and uncertainty is the same for an entire vegetation community.
- Monte Carlo simulation is valuable for modeling and mapping the
 uncertainty in corrected DEMs. The Monte Carlo modeling technique can make the estimations of the true elevations more reliable
 for an end user's needs because it combines the bias and uncertainty
 related to the underlying data into the final corrected DEM products.
 Additionally, Monte Carlo can provide error maps and supportive
 tables to compliment the model accuracy assessment.
- The object-based LiDAR correction approach has potential to better assist future research in generating more accurate and precise DEMs. The robustness of these techniques should be explored in other applications (e.g. Water Table Elevation Model (WTEM) generation) and ecosystems and urban areas. With the advancement of UAV data acquisition and derived measurements, simultaneous collection of all data sources is more achievable and may improve the object-based corrected DEM results and applications. Future research will explore the potential of object-based machine learning techniques to investigate coastal peat marsh loss by monitoring changes in small homogenous vegetation patches and elevations due to sea-level rise. It is also anticipated that the object-based correction technique will become more popular in DEM generation.

Declaration of interest

None.

Acknowledgements

This research was funded by the Everglades Foundation ForEverglades Fellowship, and the American Association of Geographers Mel Marcus Fund for Physical Geography. The opinions is this research do not necessarily reflect those of the Everglades Foundation or AAG. We also thank the helpful and friendly staff at Everglades National Park. This material was developed in collaboration with the Florida Coastal Everglades Long-Term Ecological Research program under National Science Foundation Grant No. DEB-1237517.

Appendix A. Supplementary data

Supplementary data to this article can be found online at https://doi.org/10.1016/j.envsoft.2018.11.003.

References

Aha, D., Kibler, D., 1991. Instance-based learning algorithms. Mach. Learn. 6, 37–66.Belgiu, M., Drägut, L., 2016. Random forest in remote sensing: a review of applications and future directions. ISPRS J. Photogrammetry Remote Sens. 114, 24–31.

Benz, U.C., Hofmann, P., Willhauck, G., Lingenfelder, I., Heynen, M., 2004. Multiresolution, object- oriented fuzzy analysis of remote sensing data for GIS-ready information. ISPRS J. Photogrammetry Remote Sens. 58, 239–258.

Blaschke, T., 2010. Object based image analysis for remote sensing. ISPRS J. Photogrammetry Remote Sens. 65, 2–16.

Breiman, L., 2001. Random forests. Mach. Learn. 45 (1), 5-32.

Buffington, K.J., Dugger, B.D., Thorne, K.M., Takekawa, J.Y., 2016. Statistical correction of lidar- derived digital elevation models with multispectral airborne imagery in tidal marshes. Rem. Sens. Environ. 186, 616–625.

Cahoon, D., Lynch, J., 1997. Vertical accretion and shallow subsidence in a mangrove forest of southwestern Florida, U.S.A. J. Mangroves Salt Marshes 1 (3), 173–186.

Chirici, G., Mura, M., McInerney, D., Py, N., Tomppo, E.O., Waser, L.T., Travaglini, D., McRoberts, R.E., 2016. A meta-analysis and review of the literature on the k-nearest

- neighbors technique for forestry applications that use remotely sensed data. Rem. Sens. Environ, 176, 282–294.
- Clough, J.M., Polaczyk, A., Propato, M., 2016. Modeling the potential effects of sea-level rise on the coast of New York: Integrating mechanistic accretion and stochastic uncertainty. Environ. Model. Software 84, 349–362.
- Craft, C.B., Richardson, C.J., 1993. Peat accretion and N, P, and organic C accumulation in nutrient-enriched and unriched Everglades peatlands. Ecol. Appl. 3, 446–458.
- Criminisi, A., Shotton, J., Konukoglu, E., 2011. Decision forests: A unified framework for classification, regression, density estimation, manifold learning and semi-supervised learning. Found. Trends Comput. Graph. Vis. 7 (2–3), 81–227.
- Cooper, H.M., Zhang, C., Selch, D., 2015. Incorporating uncertainty of groundwater modeling in sea-level Rise assessment: A case study in South Florida. Climatic Change 129 (1–2), 281–294.
- Cooper, H.M., Fletcher, C.H., Chen, Q., Barbee, M.M., 2013. Sea-level rise vulnerability mapping for adaptation decisions using LiDAR DEMs. Prog. Phys. Geogr. 37 (6).
- Cooper, H.M., Chen, Q., 2013. Incorporating uncertainty of future sea-level rise estimates into vulnerability assessment: A case study in Kahului, Maui. Climatic Change 121, 635–647.
- Desmond, D.G., 2003. Measuring and Mapping the Topography of the Florida Everglades for Ecosystem Restoration. US Geological Survey Fact Sheet, Reston, VA 021-03.
- Dronova, I., 2015. Object-based image analysis in wetland research: a review. Rem. Sens. 7, 6380–6413.
- Enwright, N.M., Wang, L., Borchert, S.M., Day, R.H., Feher, L.C., Osland, M.J., 2018. The impact of LiDAR elevation uncertainty on mapping intertidal habitats on barrier islands. Rem. Sens. 10 (1), 5. https://doi.org/10.3390/rs10010005.
- Gesch, D., Oimoen, M.J., Evans, G.A., 2014. Accuracy Assessment of the US Geological Survey National Elevation Dataset, and Comparison with Other Large-area Elevation Datasets: SRTM and ASTER. U.S. Geological Survey Open-File Report 2014-1008. pp. 10. https://doi.org/10.3133/ofr20141008.
- Graham, C., Talay, D., 2013. Stochastic Simulation and Monte Carlo Methods. Springer-Verlag Berlin Heidelberg.
- Hall, M.A., Frank, E., Holmes, G., Pfahringer, B., Reutemann, P., Witten, I.H., 2009. The WEKA data mining software: An update. SIGKDD Explor 11, 10–18.
- Hall, M.A., 1998. Correlation-based Feature Subset Selection for Machine Learning. (Hamilton, New Zealand).
- Henman, J., Poulter, B., 2008. Inundation of freshwater peatlands by sea-level rise:
 Uncertainty and potential carbon cycle, J. Geophys. Res. 113, G01011.
- Hladik, C., Alber, M., 2012. Accuracy assessment and correction of a LiDAR-derived salt marsh digital elevation model. Rem. Sens. Environ. 121, 224–235.
- Holmes, K.N., Chadwick, O., Kyriakidis, P., 2000. Error in USGS 30-meter digital elevation model and its impact on terrain modelling. J. Hydrol. 233, 154–173.
- Jensen, J.R., 2015. Introductory Digital Image Processing: a Remote Sensing Perspective, fourth ed. Prentice Hall Series in Geographic Information Science.
- Johnson, B., Xie, Z., 2011. Unsupervised image segmentation evaluation and refinement using a multiscale approach. ISPRS J. Photogrammetry Remote Sens. 66, 473–483.
- Jones, J.W., Desmond, G.B., Henkle, C., Glover, R., 2012. An approach to regional wet-land digital elevation model development using a differential global positioning system and a custom-built helicopter-based surveying system. Int. J. Rem. Sens. 33 (2), 450–465.
- Klemas, V.V., 2015. Coastal and environmental remote sensing from Unmanned Aerial Vehicles: An overview. J. Coast Res. 31 (5), 1260–1267.
- Leica Geosystems, 2007. Leica ALS50 II Airborne Laser Scanner Product Specifications. http://www.nts-info.com/inventory/images/ALS50-II.Ref.703.pdf.
- Leica Geosystems, 2008. Leica GPS1200 + Series Technical Data. http://www.leica-geosystems.se/se/gps_1200_glonass_150dpi.pdf.
- Lodge, T.E., 2010. The Everglades Handback: Understanding the Ecosystem, third ed. Taylor and Francis Group, Boca Raton.
- Mas, J.F., Flores, J.J., 2008. The application of artificial neural networks to the analysis of Remotely sensed data. Int. J. Rem. Sens. 29, 617–663.
- McClure, A., Liu, X.H., Hines, E., Ferner, M.C., 2016. Evaluation of error reduction techniques on a LiDAR-derived salt marsh digital elevation model. J. Coast Res. 32 (2), 424–433.
- Medeiros, S., Hagen, S., Weishampel, J., Angelo, J., 2015. Adjusting LiDAR-derived Digital Terrain Models in coastal marshes based on estimated aboveground biomass density. Rem. Sens. 7, 3507–3525.
- Morris, J.T., Porter, D., Neet, M., Noble, P.A., Schmidt, L., Lapine, L.A., Jensen, J.R., 2005. Integrating LIDAR elevation data, multi-spectral imagery, and neural network modeling for marsh characterization. Int. J. Rem. Sens. 26 (23), 5221–5234.
- Mountrakis, G., Im, J., Ogole, C., 2011. Support vector machines in remote sensing: A review. ISPRS J. Photogrammetry Remote Sens. 66, 247–259.
- National Digital Elevation Program (NDEP), 2004. Guidelines for digital elevation data, Version 1.0. http://www.ndep.gov/NDEP_Elevation_Guidelines_Ver1_10May2004. pdf.
- NOAA, 2013. Estimation of vertical uncertainties in VDatum. Retrieved from: http://vdatum.noaa.gov/docs/est_uncertainties.html.
- NRC, 2014. Progress toward Restoring the Everglades: the Fifth Biennial Review. The National Academies Press, Washington DC.
- Rogers, J.N., Parrish, C.E., Ward, L.G., Burdick, D.M., 2016. Assessment of elevation uncertainty in salt marsh environments using discrete-return and full waveform lidar. J. Coast. Res. 76, 107–122 Special Issue.
- Rogers, J.N., Parrish, C.E., Ward, L.G., Burdick, D.M., 2018. Improving salt marsh digital elevation model accuracy with full-waveform and nonparametric predictive modeling. Estuar. Coast Shelf Sci. 202, 193–211.
- Rosso, P.H., Ustin, S.L., Hastings, A., 2003. Use of LiDAR to produce high resolution marsh vegetation and terrain maps. In: Presentation at: the Three Dimensional Mapping from InSAR and LiDAR Workshop. ISPRS, Portland, OR.

- Rosso, P.H., Ustin, S.L., Hastings, A., 2006. Use of lidar to study changes associated with Spartina invasion in San Francisco Bay Marshes. Rem. Sens. Environ. 100, 295–306.
- Sadro, S., Buhl-Gastil, M., Melack, J., 2007. Characterizing patterns of plant distribution in a southern California salt marsh using remotely sensed topographic and hyperspectral data and local tidal fluctuations. Rem. Sens. Environ. 110, 226–239.
- Schmid, K.A., Hadley, B.C., Wijekoon, 2011. Vertical accuracy and use of topographic LiDAR data in coastal marshes. J. Coast Res. 27, 116–132.
- Shevade, S.K., Keerthi, S.S., Bhattacharyya, C., Murthy, K.R.K., 1999. Improvements to the SMO algorithm for SVM regression. IEEE Trans. Neural Network. 11 (5), 1188-1193
- Trimble, 2017. eCognition Developer 9.3 User Guide.
- Wechsler, S.P., Kroll, C.N., 2006. Quantifying DEM uncertainty and its effect on topographic parameters. Photogramm. Eng. Rem. Sens. 72, 1081–1090.
- Zhang, C., 2014. Combining hyperspectral and LiDAR data for vegetation mapping in the Florida Everglades. Photogramm. Eng. Rem. Sens. 80, 733–743.
- Zhang, C., Denka, S., Cooper, H., Mishra, D.R., 2018. Quantification of sawgrass marsh aboveground biomass in the coastal Everglades using object-based ensemble analysis and landsat data. Rem. Sens. Environ. 204, 366–379.
- Zhang, K., 2011. Analysis of non-linear inundation from sea-level rise using LiDAR data: A case study for South Florida. Climatic Change 106, 537–565.